RSC Advances

ROYAL SOCIETY OF CHEMISTRY

www.rsc.org/advances

Modulated Photophysics and Rotational-Relaxation Dynamics of Coumarin 153 in Nonionic Micelles: The Role of Headgroup Size and Tail Length of the Surfactants

Bijan K. Paul, Narayani Ghosh and Saptarshi Mukherjee*

Department of Chemistry, Indian Institute of Science Education and Research Bhopal, Indore By Pass Road, Bhauri, Bhopal 462066, Madhya Pradesh, India

*To whom correspondence should be addressed: saptarshi@iiserb.ac.in.

Abstract

Here, the effect of variation of the headgroup size and the alkyl tail length of nonionic surfactants on the photophysics and rotational-relaxation dynamics of the laser dye coumarin 153 (C153) has been explored. The variation in the headgroup size, that is, poly(ethylene oxide) (PEO) chain length of the nonionic micellar systems has been implemented by choice of surfactants belonging to Triton X family whereas the surfactants from the Tween family provides access to variation of the tail length (alkyl chain) of the surfactants. Our spectroscopic study reveals remarkable influence on the photophysics of C153 upon binding with the micelles. The strength of dye-micelle binding interaction is found to be enormously governed by the variation of the headgroup size and the length of the tail of the surfactants. To this end, the dye-micelle binding interaction has been quantitatively assayed from emission studies and prudently interpreted based on the micellar hydration model. Estimation of micropolarity of the dye binding site is further employed to corroborate this argument. Further, all these lines of arguments are effectively substantiated from time-resolved fluorescence experiments with particular emphasis on modulation of rotational dynamics of the dye within the micellar microheterogeneous environments.

Keywords: Coumarin 153; Nonionic micelle; Varying headgroup and tail; Rotational dynamics, Micellar hydration.

1. Introduction

Over the past few years, self-organization of various types of molecular assemblies have captured immense attention in widespread arenas of research in chemistry and biology.[1-3] The broad-spectrum of applications of various organized assemblies, e.g., micelles, cyclodextrins, vesicles and so forth has provided the impetus for the notable thrust of research surrounding them.[1-11] Amphiphilic surfactant molecules self-aggregate to form micellar assemblies which have been central to extensive research activities for years particularly in the context of 'host-guest' chemistry in which a self-organized molecular assembly, the host, can accommodate a suitable guest without forming covalent bonds. This intriguing characteristic of 'host-guest' complexation has triggered potential research prospects including applications in targeted drug delivery, development of energy storage devices, miniature model systems for mimicking the mode of action of enzymes, simpler model system for mimicking the complex biological membrane and so forth.[1-12]

The present work is focused on studying the differential interactions of an environment sensitive molecular probe, namely, coumarin 153 (C153) with a series of nonionic micellar systems with varying poly(ethylene oxide) (PEO) chain length (within Triton X series of nonionic surfactants) and alkyl chain length (within Tween series of nonionic surfactants) (the chemical structures are illustrated in Scheme 1. A simplified paradigm depicting the structures of the micellar units is presented in the Supplementary Information (SI), Scheme S1).[11] The variation in the PEO/alkyl chain length of the surfactant molecules is expected to influence the compactness of the headgroup arrangement of the micellar units[13-15] and hence the degree of water penetration to the palisade layer of the micelles. In the present program, we have used C153 as a molecular reporter which binds to the palisade layer of the studied micellar systems and monitored the spectral changes of the dye due to change in PEO chain length and alkyl chain

length. C153 is known to exhibit intramolecular charge transfer (ICT) characteristics as reflected

through remarkable sensitivity of spectral properties to solvent polarity,[16] which has

subsequently paved the way for extensive application of C153 as a molecular reporter for a host

of biological, biomimicking, and supramolecular assemblies.[16-19] Though the structural aspects,

namely, size, shape, and hydration of nonionic micelles as a function of the PEO and alkyl chain

length have been extensively addressed in the literature,[13,14,20,21] the lacuna surrounding the

water-micelle interactions are yet far from being completely resolved. The main objective of the

present study involves our endeavors toward unfolding the role of the headgroup size and alkyl

tail length in governing the interaction of the environment sensitive probe molecule C153 with

the nonionic micellar systems.

Scheme 1: Chemical Structures of (a) Coumarin 153 (C153), and (b) Tween 20 and (c) Triton X Surfactants

(a) Coumarin 153 (C153)

(b) $(x + y + z + w = 20)$

(c)
n = 7.5 in TX114
n = 9.5 in TX100
n = 16 in TX165
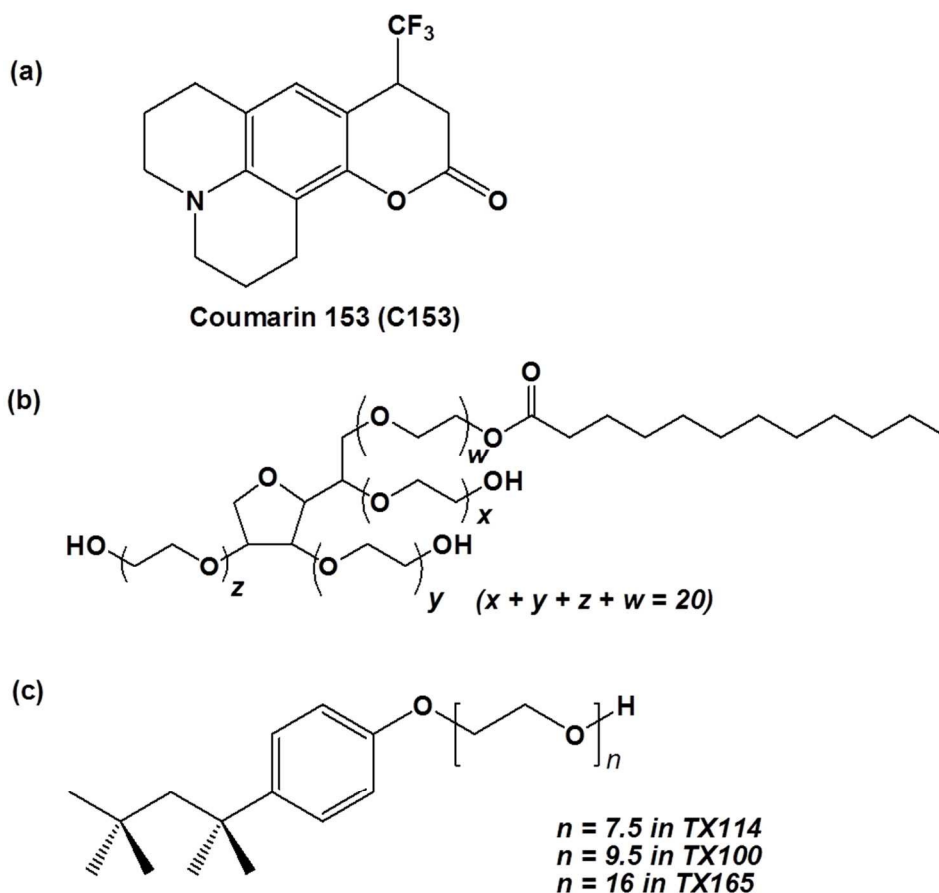
2. Experimental Section

2.1. Materials

Coumarin 153 (C153, Scheme 1) and the surfactants from Triton X (TX) series (namely, TX165, TX100, and TX114), and Tween (TW) series (namely, TW20, TW40, and TW60) were used as received from Sigma-Aldrich, USA. Tris buffer was purchased from Sigma-Aldrich, USA and 0.01 M Tris-HCl buffer of pH 7.4 was prepared from it in deionized triply distilled Milli pore water (Milli-Q water purification system).

2.2. Instrumentations and Methods

Steady-State Spectral Measurements: The absorption and fluorescence emission spectra were acquired on a Cary 100 UV-vis spectrophotometer, and Fluorolog 3-111 fluorometer, respectively. All spectroscopic measurements were performed with freshly prepared solutions containing a low concentration of the dye (~ 2.0 µM) in order to avoid inner-filter effects. Appropriate spectral background corrections were done with a similar set of solutions omitting the dye.

Steady-State Fluorescence Anisotropy: Steady-state fluorescence anisotropy (*r*) measurements were carried out on Fluorolog 3-111 fluorometer. The fluorescence anisotropy (*r*) is defined as:[22]

$$r = \frac{I_{VV} - G.I_{VH}}{I_{VV} + 2.GI_{VH}} \tag{1}$$

$$G = \frac{I_{HV}}{I_{HH}} \tag{2}$$

where, I_{VV} and I_{VH} denote emission intensities collected respectively at vertical and horizontal emission polarizations following excitation through a vertical polarization. The correction factor for detector sensitivity of the instrument (*G*) is defined through equation 2.

Time-Resolved Measurements: Fluorescence lifetimes were obtained by the method of Time-Correlated Single Photon Counting (TCSPC) following excitation of the samples at $\lambda_{ex} = 405$ nm (IBH-NanoLED-405L) using picosecond diode and the signals were collected using a Hamamatsu MCP Photomultiplier (Model R-3809U-50) at the magic angle polarization of 54.7° in order to eliminate any considerable contribution from fluorescence depolarization.[22,23] The decays were deconvoluted on DAS-6 decay analysis software. The average lifetime $\langle \tau_f \rangle$ was calculated using the following equation:[22,23]

$$\langle \tau_f \rangle = \sum_i \alpha_i \tau_i \tag{3}$$

where, α_i represents the normalized amplitude of the ith decay time constant, τ_i.[22,23]

For time-resolved fluorescence anisotropy decay measurements, the polarized fluorescence decays for parallel $[I_\parallel(t)]$ and perpendicular $[I_\perp(t)]$ emission polarizations were collected following excitation by vertically polarized light. The anisotropy decay function, $r(t)$, was then constructed according to the following relationship:[22,23]

$$r(t) = \frac{I_\parallel(t) - G.I_\perp(t)}{I_\parallel(t) + 2.G.I_\perp(t)} \tag{4}$$

The correction factor, G, was determined from long time tail matching technique.[23]

3. Results and Discussion

3.1. Steady-State Spectral Study

In aqueous buffer medium C153 shows a broad, structureless absorption band at $\lambda_{abs} \sim 425$ nm. In all the studied micellar systems the absorption profile of C153 is found to be little blue-shifted with slight enhancement of maximum absorbance as displayed in Figure 1 for the representative cases of Tween 20, and Triton X 165. This indicates that C153 experiences a

reduced polarity in the ground-state within the micellar environment in comparison to that in aqueous buffer medium.[16]
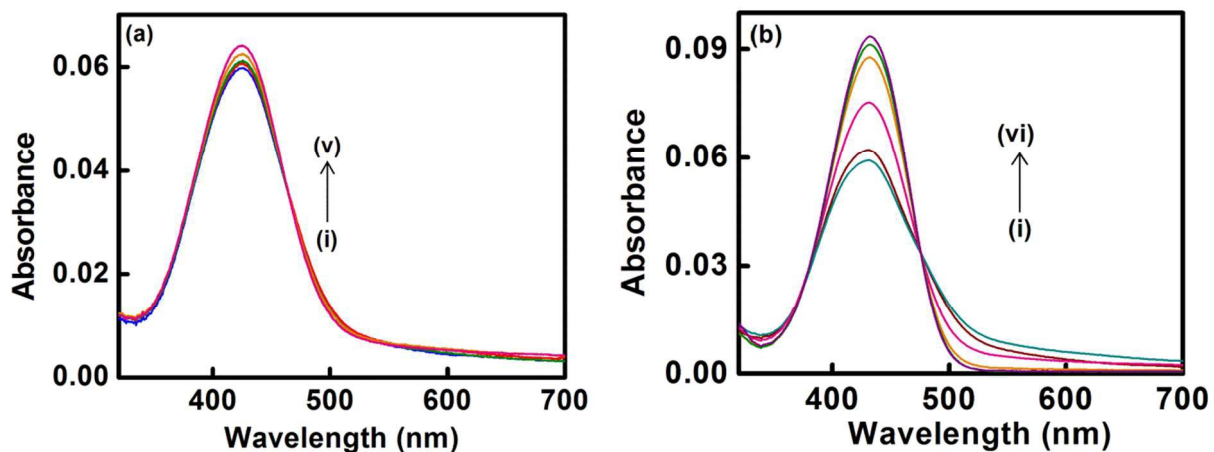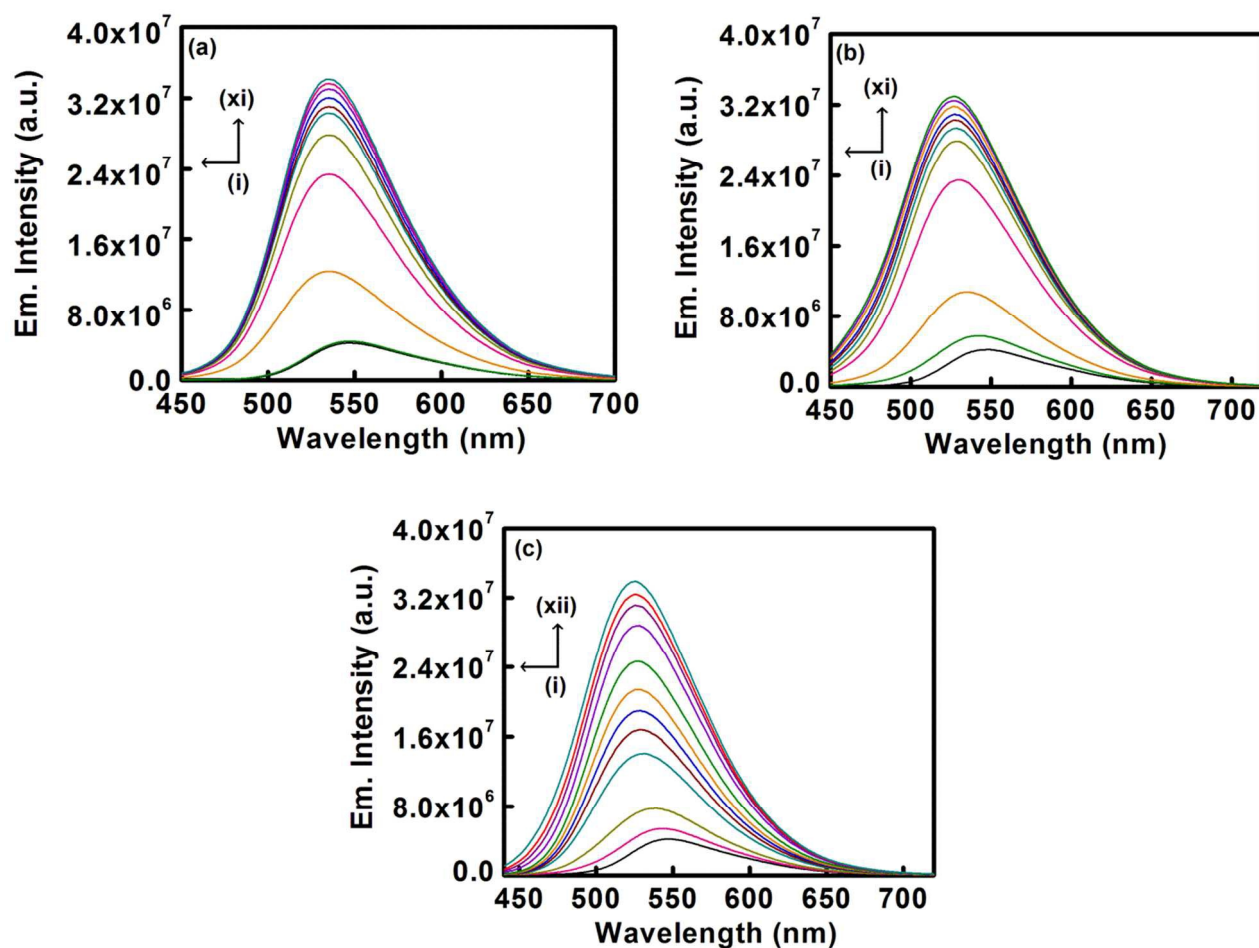

Figure 1: *Examples of absorption profiles of C153 with added (a) TW20, and (b) TX165. Curves (i) → (v) represent 0, 6, 16, 20, 30 μM TW20 in (a), and Curves (i) → (vi) represent 0, 1, 1.5, 2, 2.5, 3.5 mM TX165 in (b).*

The occurrence of interaction of C153 with the nonionic micellar systems is more dramatically reflected on the medium polarity-sensitive emission profile of the dye. As displayed in Figures 2 and 3, the emission profile of C153 undergoes remarkable modification upon addition of the nonionic surfactants in terms of a large blue-shift ($\lambda_{em} \sim$ 548 nm in aqueous buffer, $\sim$ 536 nm in TW20, $\sim$ 535 nm in TW40, $\sim$ 533 nm in TW60, and $\sim$ 525 nm in TX114, $\sim$ 527 nm in TX100, $\sim$ 535 nm in TX165) coupled with a significant increase in emission intensity in all the studied micellar assemblies. This blue-shift clearly indicates that the dye molecule senses a lower polarity within the micellar microhetrogeneous environments compared to bulk aqueous buffer phase. The enhancement of fluorescence intensity probably suggests the impartation of motional restriction on the dye molecules leading to reduction of nonradiative decay rates and hence a consequent increase of radiative decay channel as manifested through

7

the enhanced fluorescence yield. This argument is reinforced in a forthcoming section. The narrowing of the emission profile of C153 (Figures 2 and 3) within the micelle-bound state as compared to that in aqueous buffer solution further points out the occurrence of the C153-micelle interaction.
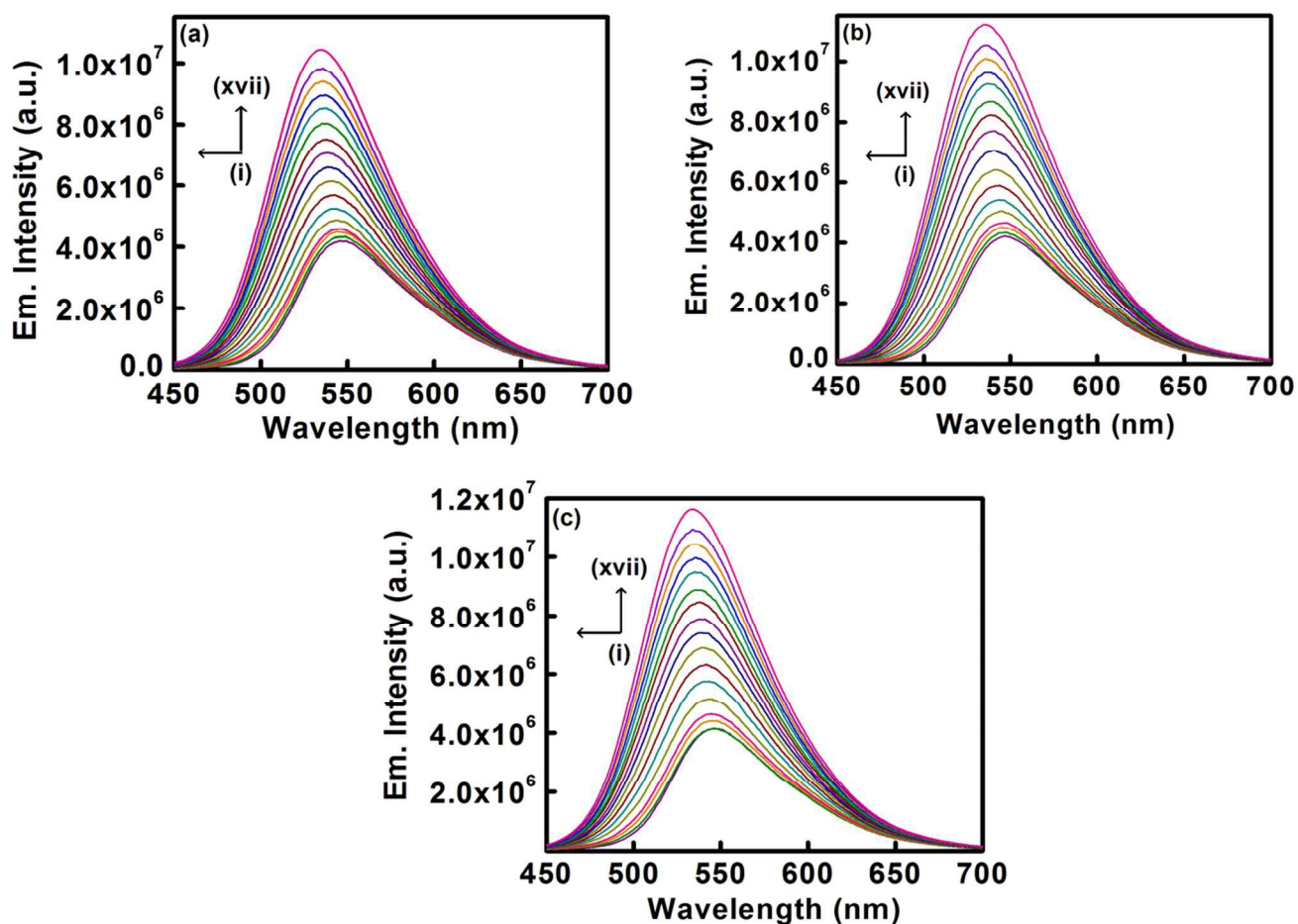
Figure 2: Examples of emission profiles of C153 with added (a) TW20, (b) TW40, and (c) TW60 in aqueous buffer medium. Curves (i) → (xvii) represent 0, 2, 4, 6, 10, 14, 18, 22, 26, 30, 34, 38, 42, 46, 50, 54, 60 μM TW20 in (a), curves (i) → (xvii) represent 0, 1, 2, 3, 5, 7, 9, 11, 13, 15, 17, 19, 21, 23, 25, 27, 30 μM TW40 in (b), and curves (i) → (xvii) represent 0, 1, 2, 3, 5, 7, 9, 11, 13, 15, 17, 19, 21, 23, 25, 27, 30 μM TW60 in (c).

Figure 3: *Examples of emission profiles of C153 with added (a) TX165, (b) TX100, and (c) TX14 in aqueous buffer medium. Curves (i) → (xi) represent 0, 1, 1.5, 2, 2.5, 3, 3.5, 4, 6, 8, 10 mM TX165 in (a), curves (i) → (xi) represent 0, 0.25, 0.31, 0.38, 0.44, 0.5, 0.56, 0.63, 0.69, 0.75, 0.81 mM TX100 in (b), and curves (i) → (xii) represent 0, 0.25, 0.31, 0.38, 0.44, 0.5, 0.56, 0.63, 0.75, 0.88, 1, 1.63 mM TX114 in (c).*

3.2. Assessing of the Probable Location of C153 within the Nonionic Micelles from Micropolarity Study

The micropolarity of the immediate vicinity of C153 inside the micelle-encapsulated state can be assayed by comparing the spectroscopic properties of C153 in the environment with those in bulk solvents/ solvent mixture of known polarity. Although such comparative method does not

claim to yield a precise determination of the polarity of a given microhetrogeneous environment in relation to that of a bulk homogeneous fluid, the results are, in general, reliable.[1,24-26] Thus, the spectroscopic properties of C153 is monitored in a solvent mixture of water and 1,4-dioxane having known polarity values depending on the relative compositions. (Figure S1 in the SI). The polarity equivalent index, $E_T(30)$, for water/1,4-dioxane mixture is taken from the literature.[26] A calibration curve is then constructed by observing the variation of the emission wavelength of C153 against the polarity index, $E_T(30)$ (Figure S1 in SI). Now, the polarity of the dye microenvironment within the micellar assemblies is determined by direct interpolation of the emission wavelength value of micelle-bound C153 on the calibration curve, Figure 4 (a detailed description of the protocol is mentioned in the SI). The as-obtained micorpolarity values in various micellar environments are collected Table 1.
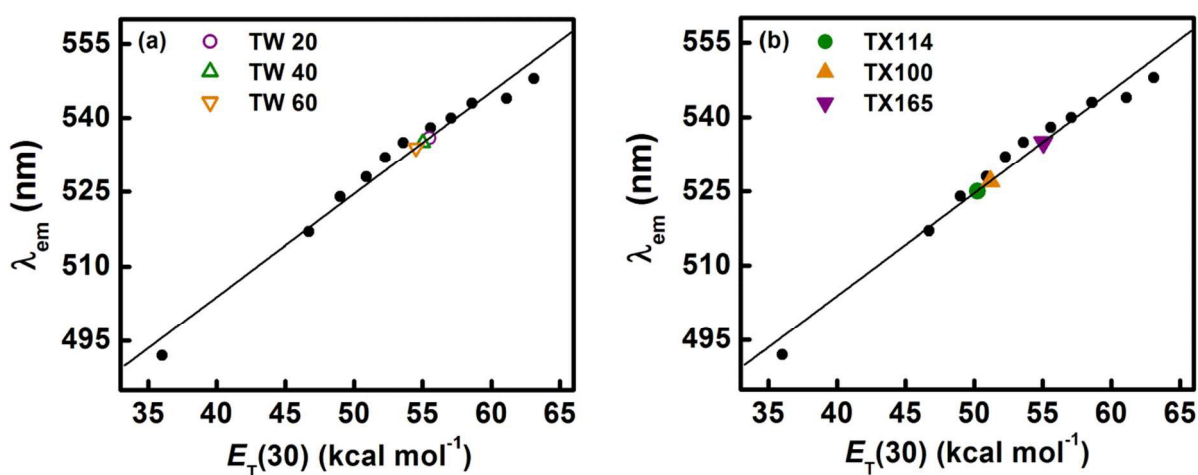
Figure 4: *Plot of variation of λ_{em} (nm) of C153 with polarity equivalent parameter $E_T(30)$ (kcal mol^{-1}) in different compositions of water/1,4-dioxane reference solvent mixture. The polarity of the dye binding site in micellar environments is indicated on the calibration curve as specified in the figure legends for Tween series in panel a (TW20: –○–, TW40: –△–, and TW60: –▽–) and Triton X series in panel b (TX114: –●–, TX100: –▲–, and TX165: –▼–). The goodness of the linear fit is judged by the correlation coefficient, $r^2 = 0.99$.*

Table 1: Binding constant (K), and free energy change (ΔG) for C153-micelle binding interaction. The micropolarity values on $E_T(30)$ scale at the dye binding sites within the nonionic micellar environments, CMCs, and the hydrodynamic radii (r_h) of the micellar systems are also indicated

System	K	ΔG (kJ mol^{-1})	$E_T(30)$ (kcal mol^{-1})	CMC	r_h (nm)
Tween 20	$(9.7 \pm 1.1) \times 10^5$	- 33.6 ± 0.25	55.5	12 μM	4.8
Tween 40	$(5.5 \pm 1.3) \times 10^6$	- 37.8 ± 0.51	55.0	11 μM	5.0
Tween 60	$(6.4 \pm 1.4) \times 10^6$	- 38.2 ± 0.48	54.5	10 μM	8.4
Triton X 165	$(1.4 \pm 0.5) \times 10^5$	- 28.8 ± 0.76	55.1	0.25 mM	3.8
Triton X 100	$(4.1 \pm 1.1) \times 10^5$	- 30.8 ± 0.68	51.2	0.10 mM	4.1
Triton X 114	$(10.5 \pm 1.5) \times 10^5$	- 33.8 ± 0.32	50.2	0.14 mM	4.5

In general, the micropolarity of C153 binding sites within the micellar assemblies is found to be considerably lower than that of aqueous buffer phase ($E_T(30)$ = 63.1 kcal mol^{-1})[26] while having striking similarity to that of methanol solvent ($E_T(30)$ = 55.5 kcal mol^{-1}).[26] This in turn appears to conform to a probable location of the dye in the palisade layer of the micellar systems.[28,29] Within the Tween series, the dye microenvironment is found to be most polar in Tween 60 and least in Tween 20 through Tween 40 being in between, that is, the polarity of the dye microenvironment decreases with increasing alkyl chain length of the Tween series micelles. However, a reverse trend is noted within the Triton X series, that is, the polarity of the dye microenvironment increases with PEO chain length, being maximum in Triton X165, and minimum in Triton X114. The change in polarity of the dye microenvironment thus occurs in the order: TW20 < TW40 < TW60 within the Tween series, and TX114 < TX100 < TX165 within the Triton X series. This observation can be rationalized on the grounds of the water penetration

model into a micellar structure. The extent of water penetration to micellar units is enormously governed by the compactness of the headgroup arrangement; less compact headgroup being more vulnerable toward water penetration. Increasing degree of micellar compactness and hence decreasing degree of water penetration with increase in alkyl chain length thus justifies the aforementioned trend of polarity along the Tween series micelles. On the other hand, with increase in PEO chain length the micelle undergoes greater extent of water penetration (reduced headgroup compactness) which accounts for the aforementioned trend of polarity along the Triton X series.[30,31] The results of micropolarity estimation around the microenvironment of the micelle-bound dye are found to be strongly substantiated from fluorescence anisotropy measurement, discussed in an upcoming section.

Further, it is pertinent here to justify the use of water/1,4-dioxane mixture as the reference solvent mixture for micropolarity determination over the use of water/alcohol mixture. Since the estimated micropolarity values for micelle-encapsulated C153 are apparently close to those of alcoholic solvents (e.g., MeOH, EtOH: having $E_T(30)$ (kcal mol^{-1}) = 55.5, 51.9, respectively),[26] the use of water/alcohol mixture for micropolarity determination is rationally avoided as this would have led to an estimated $E_T(30)$ value within the micelles to hover around the end of the calibration curve. On the contrary, application of water/1,4-dioxane solvent mixture can eliminate this difficulty as this covers a wider range of polarity and thereby ensuring a better reliability of the results.

3.3. C153-Micelle Binding

The C153-micelle binding constant (K) is determined by the method described by Almgren et al.[32] using the following relationship:

$$\frac{1}{I_x - I_0} = \frac{1}{I_\infty - I_0} + \frac{1}{K[M]} \times \frac{1}{I_\infty - I_0} \qquad (5)$$

Here, I_0, I_x and I_α represent, respectively, the fluorescence intensity of the fluorophore in the absence of surfactant, at an intermediate concentration of surfactant, and under conditions of saturation of interaction.

The micellar concentration [M] is expressed as:

$$[M] = \frac{[S] - CMC}{N_{agg}} \tag{6}$$

Here, [S] represents the surfactant concentration, CMC is the critical micellar concentration and N_{agg} is the aggregation number of the surfactant.

The double reciprocal plots of $1/[I_x - I_0]$ versus $1/[M]$ leading to the estimation of C153-micelle binding constants in all the studied micellar environments following equation 5 are displayed in Figures S2 and S3 of the SI, and the free energy change (ΔG) for the binding process has been subsequently evaluated from the relationship:

$$\Delta G = -RTlnK \tag{7}$$

The negative free energy change evidences the spontaneity of the dye-micelle binding process in all the cases under investigation (Table 1).[33-37] Of particular interest in the present context is to note the relative orders of magnitude of the binding constants in the two different series of micellar assemblies (Table 1). The size of the headgroup (Triton X series) and alkyl tail length (Tween series) of the micellar assemblies are found to have profound influence on the C153-micelle binding constant (K) following in order as: $K_{TX165} < K_{TX100} < K_{TX114}$ (that is, an inverse relationship with the PEO chain length within the Triton X series) and $K_{TW20} < K_{TW40} < K_{TW60}$ (that is, proportionate variation with the surfactant tail length within the Tween series). The CMC values as determined from the variation of emission intensity of C153 with added surfactants are assembled in Table 1 (representative examples are given in Figure S4 of the SI).

3.4. Steady-State Fluorescence Anisotropy

As depicted in Figure 5, the enhancement of fluorescence anisotropy of C153 with increasing surfactant concentration provides a clear signature for the impartation of motional restriction on the dye molecules within the micelle-entrapped state as compared to the free dye (in aqueous buffer medium).[9,10,12-23,36,38]
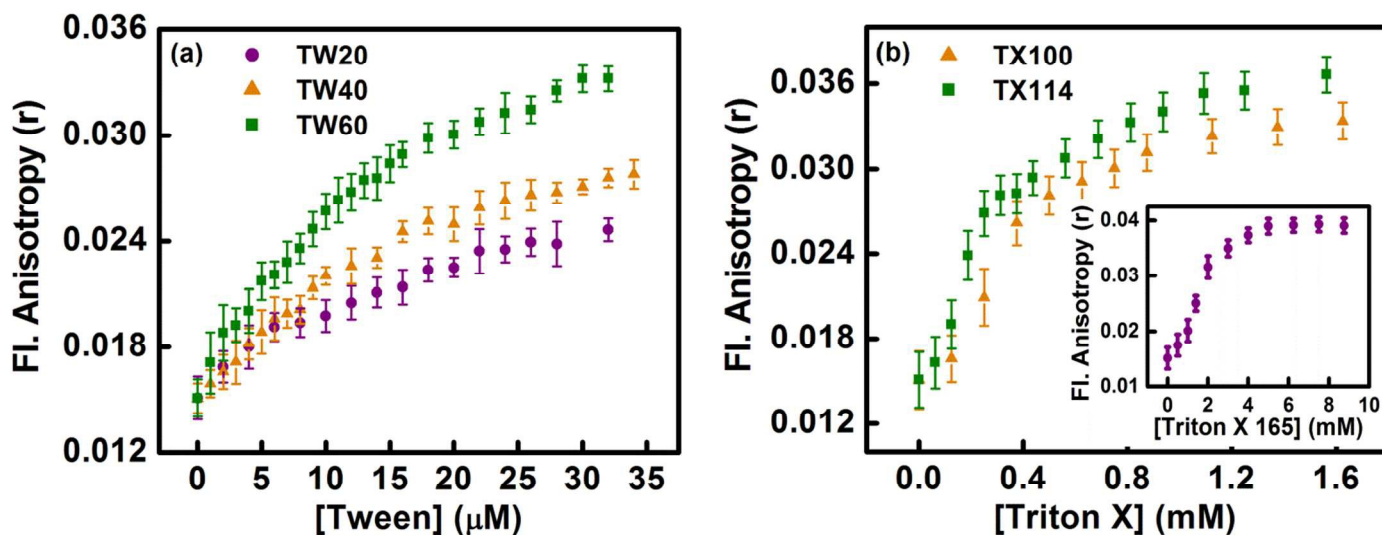
Figure 5: Variation of steady-state fluorescence anisotropy (r) of C153 as a function of (a) Tween, and (b) Triton X concentrations (the plot for TX165 is shown in the inset because of the difference in scale on the abscissa). Each data point is an average of 15 individual measurements. The error bars are within the marker symbols if not apparent.

Further, it is intriguing to note that the differential variation of fluorescence anisotropy of C153 as a function of the headgroup size or alkyl tail length of the micellar systems yields a distinct clue to assess the differential degrees of motional restriction imposed on the fluorophore. Within the Tween series the anisotropy varies as TW20 < TW40 < TW60, that is, an increasing degree of motional confinement imposed on the dye molecules with increasing length of the alkyl tail of the surfactants, while the pattern of variation is typically reversed within the Triton

X series, TX165 < TX100 < TX114, that is, the degree of motional restriction on the dye

molecules varies inversely with the size of the headgroup (PEO chain length). The variation of

fluorescence anisotropy of C153 within the micellar aggregates is thus found to bear a

commendable harmony to the pattern of variation of C153-micelle binding strength (Section

3.3). This can be rationalized on the ground of the compactness of the micellar headgroups

which increases with increasing alkyl chain length (in Tween series), and decreases with

increasing PEO chain length (in Triton X series). Thus, the micellar hydration model can be

invoked to aptly rationalize the findings. Figure 5 shows that the increment of steady-state

fluorescence anisotropy (r) of C153 with added Tween series of surfactants is regular in nature,

that is, a monotonous increase with surfactant concentration followed by saturation (Figure 5a).

Whereas, the pattern of variation with addition of Triton X series of surfactants is a bit different,

the change of anisotropy (r) is not very significant in the lower surfactant concentration regime

which is then followed by a drastic increase of anisotropy before attaining saturation and thus

conforms to a sigmoidal nature of variation (Figure 5b).

3.5. Fluorescence Decay Measurements

Representative examples of fluorescence decay transients of C153 in TW20 and TX100

micellar environments are displayed in Figure 6 (the decay transients obtained in other micellar

assemblies are displayed in Figure S5 of the SI) and the corresponding fitting parameters are

summarized in Table S1 in SI. The dye (C153) is seen to exhibit a biexponential decay pattern

both in aqueous buffer solution and the micellar systems investigated signifying a degree of

associated heterogeneity. By virtue of its intramolecular charge transfer (ICT) photophysics,

C153 is known to experience a remarkable increase of dipole moment following

photoexcitation.[16] Besides this, the fluorescent probe used C153 contains several heteroatoms so

that unequal hydration of C153 in the excited-state is also likely which adds on to the extent of

heterogeneity. Thus, the biexponential decay behavior of C153 in aqueous buffer may not be surprising and can be ascribed to the structure of the fluorescent probe. Therefore, for such heterogeneous systems, it is nontrivial to assign specific mechanistic model to individual decay components. So, instead of emphasizing on the magnitude of each decay component, we choose to use the average lifetime to study the dynamical behavior of the micelle-bound C153. In order to enable a qualitative assessment for the modulation of fluorescence decay behavior of C153 within the hydrophobic micellar environments, the data are compared with those obtained in water/1,4-dioxane mixture. The decay parameters of C153 in water/1,4-dioxane mixture are displayed in Table S2 in SI. In aqueous medium C153 exhibits a biexponential decay comprising of a major fast component and relatively slow minor component. With increasing 1,4-dioxane proportion in the mixture, that is, decreasing polarity, the contribution of the longer lifetime component increases (along with increase in average lifetime). In micelle-bound condition, C153 is found to exhibit a similar trend in fluorescence decay behavior, that is, with increase in surfactant concentration the contribution of the longer decay component increases accompanying an increase in the average lifetime (Table S1). Nevertheless, the decay behavior of C153 in micellar environment is not superimposable with that in bulk water/1,4-dioxane mixture. This is not surprising given the microheterogeneous nature of micellar environments as against the bulk homogeneous medium of water/1,4-dioxane mixture. It is seen from the data compiled in Table S3 that for Tween series, with increasing alkyl chain length the average lifetime increases while the reverse pattern is observed in the case of variation of PEO chain length within the Triton X series. For Tween series micelle with increase in alkyl chain length, the palisade layer of the micelle experiences enhanced rigidity and a consequent greater degree of hydrophobicity due to less water penetration while the reverse interaction scenario prevails for Triton X series micelles

16

with increasing PEO chain length. This accounts for the observed trend in the variation of average lifetime of C153 in the various micellar assemblies (Table S3).

      With a view to delve deeper into the modification of excited-state photophysical properties of C153 within the studied micelles, the radiative (k_r) and nonradiative (k_{nr}) decay rate constants for C153 have been estimated using the following equations[22,27] and the respective parameters are shown in Table S3:

$$k_r = \frac{\Phi_f}{\langle \tau_f \rangle} \tag{8}$$

$$k_{nr} = \frac{1}{\langle \tau_f \rangle} - k_r \tag{9}$$

where, Φ_f is the fluorescence quantum yield, and $\langle \tau_f \rangle$ is the average fluorescence lifetime. As surfactant concentration increases for all Tween and Triton X series micelles the radiative decay rate is found to increase with concomitant reduction of nonradiative decay rate.[27] These data also corroborate to the observed modifications in steady-state emission profile of C153 in the sense that an increase of k_r, and decrease of k_{nr} can be connected with the increment of emission intensity of the dye as a function of surfactant concentration.
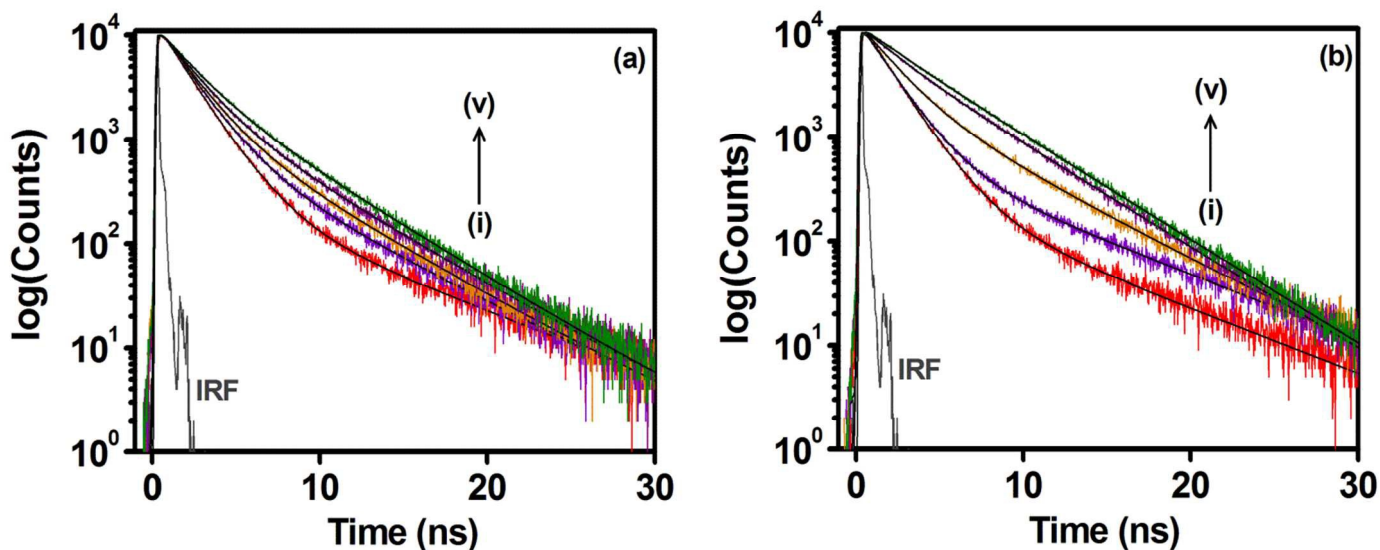
Figure 6: *Representative examples of fluorescence decay transients of C153 in (a) TW20, and (b) TX100 micellar environments. Curves (i) → (v) represent 0, 6, 22, 30, 38 μM TW20 in (a), and 0, 0.13, 0.25, 0.38, 0.5 mM TX100 in (b). IRF: instrument response function. The black solid lines are the fitted curves.*

3.6. Rotational-Relaxation Dynamics

The typical anisotropy decay profiles of C153 in various micellar assemblies are displayed in Figure 7, and the relevant rotational-relaxation dynamical parameters are summarized in Table 2.
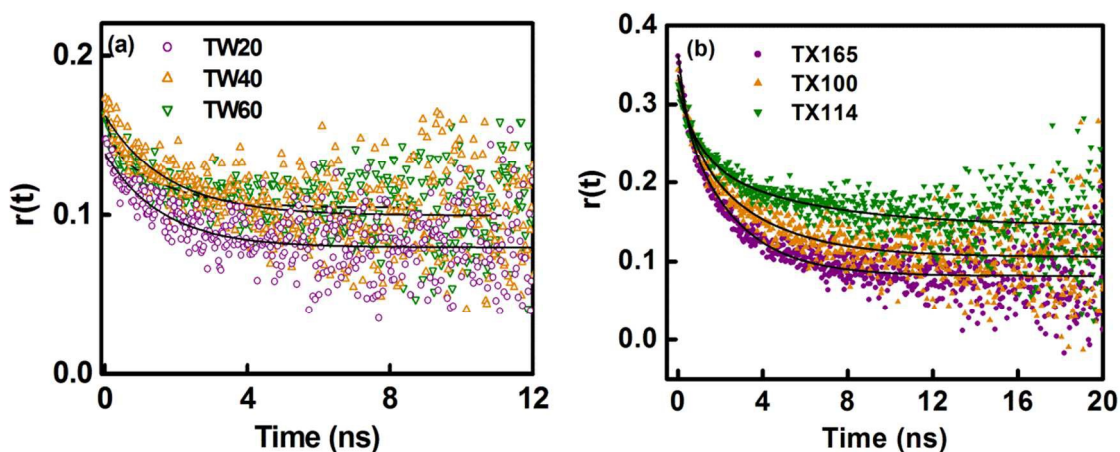
Figure 7: *Time-resolved fluorescence anisotropy decay profiles of C153 in various micellar environments of (a) Tween series (TW20: –○–, TW40: –△–, TW60: –▽–), and (b) Triton X series (TX165: –●–, TX100: –▲–, TX114: –▼–).*

Table 2: Rotational-relaxation dynamical parameters of C153 in various nonionic micellar environments

System	β	θ (± 4%) (ns)
Tween 20	1.00	1.57
Tween 40	1.00	1.75
Tween 60	1.00	1.86
Triton X 165	1.00	2.14
Triton X 100	1.00	2.54
Triton X 114	1.00	3.12

C153 is found to exhibit a monoexponential anisotropy decay in aqueous buffer as well as all the studied micellar environments. The anisotropy decay function is described as:[22]

$$r(t) = \sum_i r_0 \beta_i exp(- t/\theta_i) \tag{10}$$

in which $r_0 = \sum_i r_{0i}$ is the limiting anisotropy, β_i represents the amplitude corresponding to the ith rotational-correlation time, θ_i. The increase in rotational-relaxation time of C153 within the micelle-encapsulated state as compared to that in aqueous buffer phase (Table 2) implies that the dye molecules experience considerable rigidity within the micellar microheterogeneous environments. Further, the variation of rotational-relaxation time of the dye in different micellar environments is noteworthy in the present context. Within the Tween series, the rotational-relaxation time is found to increase with increasing alkyl chain length, while within the Triton X series with increasing PEO chain length the rotational-relaxation dynamics of the dye is found to be faster (Table 2). This pattern of observation is found to be in good agreement with other experimental findings as discussed previously based on the micellar hydration model.

Now, several arguments may be invoked to describe the monoexponential fluorescence depolarization profile of C153 within the micellar systems. The following possibilities are thus taken into consideration:[10,11,35,39-41] (i) rotation of the dye within the micellar units with no significant contribution from the rotation of the latter; (ii) rotation of the micellar unit encapsulating the dye with no significant contribution from rotation of the dye itself; and (iii) both rotations are operative. The third possibility is, however, summarily negated in view of an observed monoexponential anisotropy decay pattern of micelle-bound C153 since a biexponential decay functional can only aptly describe this possibility. Thus, in order to confirm one of the former two possibilities the rotational-relaxation time of the micellar unit (θ_m) has been estimated using the Stokes-Einstein-Debye (SED) relationship:[39,40]

$$\theta_m = \frac{4}{3}\pi r_h^3 \times \frac{\eta}{k_B T} \tag{11}$$

Here, η is the coefficient of viscosity of the medium, r_h is the hydrodynamic radius of the micellar aggregates (as obtained from DLS measurement and summarized in Table 1), k_B is the Boltzmann constant and T is the Kelvin temperature. From the calculated θ_m values the rotational-relaxation time of the micellar units is found to be remarkably higher than the corresponding fluorescence depolarization times as found in experiments. This leads to conclude that the observed rotational-relaxation dynamics of the micelle-encapsulated dye is attributable to the rotational motion of the dye only, and not the micellar units.[10,11,35,39-41]

4. Summary

The present work reports the study of interaction of the laser dye C153 with a series of nonionic micellar assemblies varying in their lengths of the headgroups (Triton X series) and the tail parts (Tween series) of the constituent surfactants. Apart from demonstrating the efficient binding interaction of C153 with all the micellar systems studied the present work reveals intriguing modifications to the photophysics of the dye as induced by the microheterogeneous

micellar assemblies. From the series of steady-state and time-resolved spectroscopic results the probable location of the dye molecule is substantiated to be in the palisade layer of all the micelles under investigation with the strength of dye-micelle interaction being enormously dependent on the alkyl chain length (within the Tween series) or the PEO chain length (within the Triton X series). Such differential interaction of the dye molecule with the micellar systems is found to be aptly rationalized on the lexicon of the micellar hydration model, that is, the varying susceptibility of micellar units to the degree of water penetration depending on the thickness of the palisade layer and hence a micellar polarity at the C153 interaction site as a function of variation in the alkyl/PEO chain length.[30,31] Our time-resolved fluorescence depolarization study reveals that the motional confinement imposed on the micelle-encapsulated dye molecules decreases with an increase in the PEO chain length while it increases with an increase in the alkyl chain length as subsequently corroborated from steady-state fluorescence anisotropy measurements.[22]

Acknowledgments

References:

(1) B. K. Paul, A. Samanta and N. Guchhait, *Langmuir*, 2010, **26**, 3214-3224.

(2) D. Panda, S. Khatua and A. Datta, *J. Phys. Chem. B*, 2007, **111**, 1648-1656.

(3) N. C. Maiti, M. M. G. Krishna, P. J. Brito and N. Periasamy, *J. Phys. Chem. B*, 1997, **101**, 11051-11060.

(4) M. V. Rekharsky and Y. Inoue, *Chem. Rev.*, 1998, **98**, 1875-1917.

(5) R. Villalonga, R. Cao and A. Fragoso, *Chem. Rev.*, 2007, **107**, 3088-3116.

(6) N. S. Bodor, Chemical aspects of drug delivery systems; D. R. Karsa, R. A. Stephenson, Eds.; Royal Society of Chemistry: London, 1996.

(7) Y. Xia, J. Rodgers, K. E. Paul and G. M. Whitesides, *Chem. Rev.*, 1999, **99**, 1823-1848.

(8) S. Hashimoto and J. K. Thomas, *J. Am. Chem. Soc.*, 1985, **107**, 4655-4662.

(9) B. K. Paul, A. Samanta and N. Guchhait, *J. Phys. Chem. B*, 2010, **114**, 6183-6196.

(10) E. L. Roberts, J. Dey and I. M. Warner, *J. Phys. Chem. A*, 1997, **101**, 5296–5301.

(11) B. K. Paul, N. Ghosh and S. Mukherjee, *J. Phys. Chem. B*, 2014, **118**, 11209-11219.

(12) C. Tanford, *Science*, 1978, **200**, 1012-1018.

(13) P. Becher, *J. Colloid Sci.*, 1961, **16**, 49-56.

(14) Y. Saito and T. Sato, *J. Phys. Chem.*, 1985, **89**, 2110-2112.

(15) V. Khorwal and A. Datta, *J. Photochem. Photobiol. A*, 2012, **250**, 99-102.

(16) R. Karmakar and A. Samanta, *J. Phys. Chem. A*, 2002, **106**, 6670-6675.

(17) C. C. Ruiz, *Photochem. Photobiol. Sci.*, 2012, **11**, 1331-1338.

(18) T. Gallavardin, M. Maurin, S. Marotte, T. Simon, A.-M. Gabudean, Y. Bretonniere, M. Lindgren, F. Lerouge, P. L. Baldeck, O. Stephan, Y. Leverrier, J. Marvel, S. Parola, O. Maury and C. Andraud, *Photochem. Photobiol. Sci.*, 2011, **10**, 1216-1225.

(19) N. Sarkar, A. Datta, S. Das and K. Bhattacharyya, *J. Phys. Chem.*, 1996, **100**, 15483-15486.

(20) T. Inoue and T. Misono, *J. Colloid and Interface Sci.*, 2008, **326**, 483-489.

(21) S. H. Chen, *Annu. Rev. Phys. Chem.*, 1986, **37**, 351-399.

(22) J. R. Lakowicz, Principles of fluorescence spectroscopy, New York: Plenum, 1999.

(23) D. V. O'Connor and D. Philips, Time-correlated single photon counting; Academic Press: London, 1984.

(24) M. E. Vazquez, J. B. Blanco and B. Imperiali, *J. Am. Chem. Soc.*, 2005, **127**, 1300-1306.

(25) A. Sytnik and M. Kasha, *Proc. Natl. Acad. Sci., USA*, 1994, **91**, 8627-8630.

(26) C. Reichardt, *Chem. Rev.*, 1994, **94**, 2319-2358.

(27) E. M. Kosower, H. Dodiuk, K. Tanizawa, M. Ottolenghi and N. Orbach, *J. Am. Chem. Soc.*, 1975, **97**, 2167-2178.

(28) M. d. M. Graciani, M. Munoz, A. Rodriguez and M. L. Moya, *Langmuir*, 2005, **21**, 3303-3310.

(29) E. M. Koswer, Reactions through charge transfer complexes. In: Taft, R. W. (ed.), Progress in Physical Organic Chemistry, vol. 3, Wiley Interscience, New York, 1965.

(30) N. Muller, Reaction kinetics in micelles, in: Cordes, E. A. (Ed.), Plennum, New York, 1973.

(31) S. Berr, R. R. M. Jones and J. S. Johnson, *J. Phys. Chem.*, 1992, **96**, 5611-5617.

(32) M. Almgren, F. Grieser and J. K. Thomas, *J. Am. Chem. Soc.*, 1979, **101**, 279-291.

(33) D. Reyman, A. Pardo and J. M. L. Poyato, *J. Phys. Chem.*, 1994, **98**, 10408-10411.

(34) M. Beljanski and M. S. Beljanski, *Exp. Cell Biol.*, 1982, **50**, 79-87.

(35) B. K. Paul and N. Guchhait, *J. Phys. Chem. B*, 2011, **115**, 10322-10334.

(36) B. K. Paul and N. Guchhait, *J. Phys. Chem. B*, 2011, **115**, 11938-11949.

(37) P. R. Bevington and D. K. Robinson, Data reduction and error analysis for the physical sciences, 2nd ed., Chapter 8; WCB/McGraw-Hill: Boston, 1992

(38) M. M. Gonzalez, J. Arnbjerg, M. P. Denofrio, R. Erra-Balsells, P. R. Ogilby and F. M. Cabrarizo, *J. Phys. Chem. A*, 2009, **113**, 6648-6656.

(39) B. K. Paul and N. Guchhait, *J. Colloid Interface Sci.*, 2011, **363**, 529-539.

(40) R. Thakur, A. Das and A. Chakraborty, *RSC Adv.*, 2014, **4**, 14335-14347.

(41) I. Vayá, J. Brazard, T. Gustavsson and D. Markovitsi, *Photochem. Photobiol. Sci.*, 2012, **11**, 1767-1773.

For "table of contents" use only
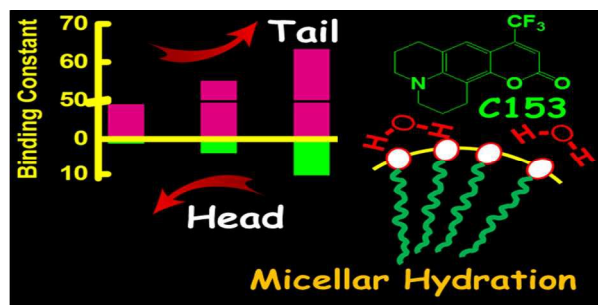
Effect of variation of the headgroup size and tail length on the photophysics and rotational dynamics of embedded dye C153